

old. In a sample of the 40 units for which there is complete data, the median errors in the roving-level condition increased by an average of only 6.3° above the larger of the median errors in the two constant-level conditions. Network performance was substantially worse, however, when we attempted to train with responses to 20-dB stimuli and test with 40-dB responses.

We compared the classification based on spike patterns with a classification based on spike counts alone. The one-layer perceptron was poorly suited to classify counts because the spike count measure has only a single dimension. Instead, we used a maximum likelihood estimator, which can be shown to be an optimal classifier (11). In that procedure, spike counts from the bootstrapped training sets were used to accumulate the spike probability distribution for each stimulus location, then counts from the test sets were classified by assigning to each count the most probable stimulus location. We could not use the maximum likelihood procedure to classify temporal spike patterns because the probability distribution for that 40-dimensional measure (corresponding to the 40 1-ms time bins) could not be estimated. The network classification of spike patterns generally outperformed any classification of spike counts. A comparison of the performance of the network in classifying spike patterns with the performance of a maximum likelihood estimator in classifying spike counts alone is shown in Fig. 3. The spike count classifier was fairly successful at identifying the correct loudspeaker (open symbols), although its performance was below the random chance level for 6 of 67 units. In contrast, the pattern classifier performed better than chance for all but one unit, and the pattern classifier surpassed the spike count classifier for 50 of 67 units (74.6%). Moreover, when the spike count classifier erred, it tended to make larger errors than did the pattern classifier, so the pattern classifier gave more responses within 50° of the correct loudspeaker for all but three units.

In the optic tectum and superior colliculus, sound locations appear to be represented by a place code in which, by virtue of the spatial tuning of single neurons, a particular sound source location maps onto a particular place within the tectal or collicular map (1). No such auditory map has been demonstrated in the cerebral cortex. Our results suggest an alternative view, in which a stimulus at nearly any location activates a diffuse population of neurons. In this view, each of the active neurons signals, with its temporal firing pattern, the approximate location of the sound source, and the precise sound source location is signalled by the concerted activity of many such neurons. Each neuron is panoramic in

that it can carry information about locations throughout 360° of azimuth. Although there are many instances in sensory physiology in which particular stimuli can be shown to be represented by the levels of activity of tuned neurons, it is unrealistic to imagine that every possible stimulus dimension is represented by a corresponding class of tuned neurons. Sound location might prove to be one example of a stimulus dimension that is represented in the cortex by a temporal firing code rather than by a place code. The temporal pattern classification that we have applied in this instance may be applicable to a variety of problems in sensory coding.

REFERENCES AND NOTES

1. E. I. Knudsen, *J. Neurosci.* 2, 1177 (1982); A. R. Palmer and A. J. King, *Nature* 299, 248 (1982); J. C. Middlebrooks and E. I. Knudsen, *J. Neurosci.* 4, 2621 (1984).
2. L. M. Optican and B. J. Richmond, *J. Neurophysiol.* 57, 162 (1987); B. J. Richmond and L. M. Optican, *ibid.* 64, 370 (1990).
3. The animal protocol was approved by the University of Florida Institutional Animal Care and Use Committee. Anesthesia was induced with isoflurane in 70% N₂O/30% O₂, then an intravenous infusion of α -chloralose (25 mg/ml in propylene glycol) was begun. The cat was transferred from the isoflurane to the α -chloralose; typically 125 to 150 mg of α -chloralose was needed. Anesthesia was maintained with supplemental injections of α -chloralose (~0.5 cm³ per hour). We monitored the level of anesthesia by monitoring heart rate with an esophageal stethoscope.
4. Spike patterns were digitized with 0.1-ms resolution, low-pass filtered below 137 Hz by convolution with a unit Gaussian impulse ($\sigma = 1$ ms), then resampled with 1-ms resolution to form an estimate of a spike density function based on 40 1-ms bins.
5. B. Efron and R. Tibshirani, *Science* 253, 390 (1991).
6. B. Widrow and M. E. Hoff, *IRE WESCON Con. Rec.* pt. 4, 96 (1960). Reprinted in J. A. Anderson and E. Rosenfeld, *Neurocomputing: Foundations of Research* (MIT Press, Cambridge, MA, 1988).
7. Efforts to configure the network with a single output unit that would generate estimated stimulus azimuth were confounded by the discontinuity in the nominal azimuth scale for loudspeakers located behind the animal. There, two loudspeakers that are only 20° apart, at -180° and +160°, correspond to a nominal difference in azimuth of 340°. In contrast, sine and cosine of azimuth are continuous across the rear midline.
8. W. M. Jenkins and R. B. Masterton, *J. Neurophysiol.* 47, 987 (1982).
9. K. H. Britten, M. N. Shadlen, W. T. Newsome, J. A. Movshon, *J. Neurosci.* 12, 4745 (1992).
10. J. C. Middlebrooks and J. D. Pettigrew, *J. Neurosci.* 1, 107 (1981); T. J. Imig et al., *J. Neurophysiol.* 63, 1448 (1990); R. Rajan et al., *ibid.* 64, 872 (1990).
11. J. Neyman and E. S. Pearson, *Philos. Trans. R. Soc. London Ser. A* 231, 289 (1933); D. M. Green and J. A. Swets, *Signal Detection Theory and Psychophysics* (Wiley, New York, 1974).
12. Supported by NIH (National Institute on Deafness and Other Communicative Disorders) and the Office of Naval Research.

3 November 1993; accepted 24 March 1994

Specification of Pore Properties by the Carboxyl Terminus of Inwardly Rectifying K⁺ Channels

Maurizio Tagliatela, Barbara A. Wible, Roberta Caporaso, Arthur M. Brown*

Inwardly rectifying potassium (K⁺) channels (IRKs) maintain the resting membrane potential of cells and permit prolonged depolarization, such as during the cardiac action potential. Inward rectification may result from block of the ion conduction pore by intracellular magnesium (Mg²⁺). Two members of this family, IRK1 and ROMK1, which share 40 percent amino acid identity, differ markedly in single-channel K⁺ conductance and sensitivity to block by Mg²⁺. The conserved H₅ regions were hypothesized to determine these pore properties because they have this function in voltage-dependent K⁺ channels and in cyclic nucleotide-gated channels. However, exchange of the H₅ region between IRK1 and ROMK1 had no effect on rectification and little or no effect on K⁺ conductance. By contrast, exchange of the amino- and carboxyl-terminal regions together transferred Mg²⁺ blockade and K⁺ conductance of IRK1 to ROMK1. Exchange of the carboxyl but not the amino terminus had a similar effect. Therefore, the carboxyl terminus appears to have a major role in specifying the pore properties of IRKs.

The predicted topology of IRKs is very different from that of voltage-dependent K⁺ channels. For IRKs, hydropathy plots suggest only two potential transmembrane segments, called M₁ and M₂ (1-4); for voltage-dependent K⁺ channels, six transmembrane segments (S₁ to S₆) have been postulated (5). Segments M₁ and M₂ are separated by a region called H₅ because of

its extensive sequence similarity with a conserved region linking the fifth and sixth transmembrane segments of voltage-dependent K⁺ channels (also called SS₁-SS₂) (6). Segment H₅ is thought to line the pore of voltage-dependent K⁺ (7), Na⁺ (8), and Ca²⁺ channels (9), as well as cyclic nucleotide-gated channels (10). Because of sequence homology, H₅ has

Fig. 1. Single-channel ramp currents of IRK1 and ROMK1 channels expressed in *Xenopus* oocytes. Single-channel ramp currents from either (A) IRK1 or (B) ROMK1 were recorded from the same patch in the cell-attached configuration (left panels), after patch excision in a Mg^{2+} -free solution (middle panels), and after the addition of 0.288 mM Mg^{2+} to the internal solution (right panels). Pipette solution: K^+ -Ringer; bath solution: iso- K^+ . The zero Mg^{2+} ramp current in IRK1 came from a fully open channel. At depolarized potentials, the probability of opening was reduced as a consequence of the intrinsic gating that is known to occur in these channels (13–17). The g_{K^+} values are expressed as slope conductance measured between -160 and -20 mV in cell-attached patches by the use of voltage steps. In our solution conditions, g_{K^+} values for IRK1 and ROMK1 are consistent with those already reported (1, 2).

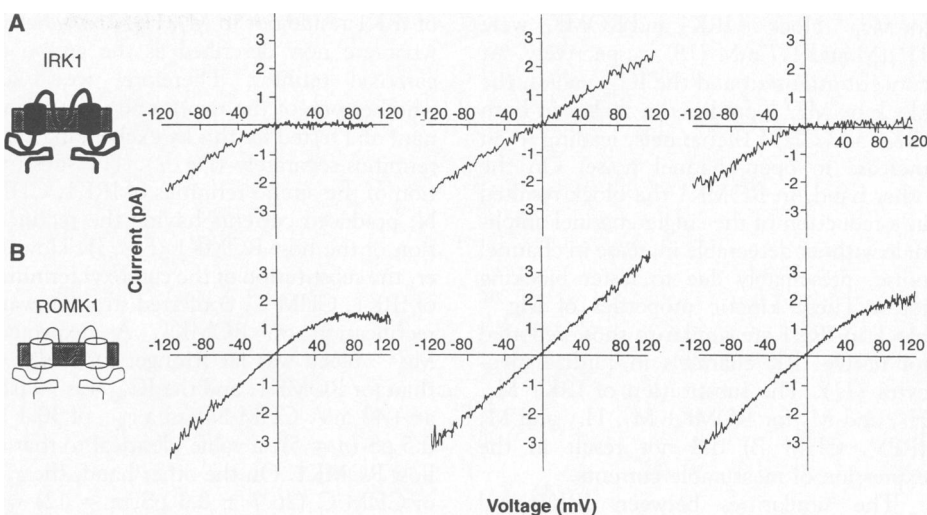


Fig. 2. Alignment of the amino acid sequences of IRK1 and ROMK1 and design of the ROMK1-IRK1 chimeric constructs. (A) The complete coding sequences of IRK1 and ROMK1, aligned and separated into five domains (amino terminus, M_1 , H_5 domain, M_2 , and carboxyl terminus) (2). Gaps are given by hyphens, and identities are given by colons. The H_5 domain includes the highlighted region, which corresponds to the region of homology with H_5 of voltage-gated K^+ channels (2), as well as the 5' and 3' flanking regions. (B) Six chimeric cDNA constructs between ROMK1 and IRK1.



been suggested to line the pore of IRKs (11).

Despite the high degree of sequence homology among IRKs, large differences exist in rectification and single-channel K^+ conductance (g_{K^+}). The IRK1 channel, cloned from a mouse macrophage cell line (2), has a g_{K^+} of 21.2 ± 0.5 pS ($n = 12$) and displays marked inward rectification in cell-attached patches (Fig. 1A, left panel) (12). On the other hand, ROMK1, an adenosine triphosphate (ATP)-regulated IRK channel cloned from the outer medulla of rat kidney cells (1), has a g_{K^+} of 31.0 ± 0.8 pS ($n = 8$) and shows modest inward rectification in cell-attached patches (Fig. 1B, left panel). In both IRK1 and ROMK1,

patch excision into a Mg^{2+} -free intracellular solution removed inward rectification (Fig. 1, A and B, middle panels); subsequent addition of 0.288 mM Mg^{2+} to the intracellular side of the patch restored the rectification properties observed in the cell-attached mode (Figs. 1, A and B, right panels). Therefore, the inward rectification is primarily due to a block by intracellular Mg^{2+} (Mg_i^{2+}) (13–17) and is strong for IRK1 and weak for ROMK1.

We investigated the molecular nature of these differences by engineering chimeric constructs between ROMK1 and IRK1 (Fig. 2) and expressing the corresponding cRNAs in *Xenopus* oocytes. The possible role of the H_5 region in Mg^{2+} block and unitary conductance was tested by the exchange of H_5 domains between the two IRKs. Substitution of the ROMK1 H_5 domain into IRK1 (CHM A) changed neither rectification (Fig. 3) nor g_{K^+} (20.2 ± 0.5 pS; $n = 12$). Just as transplantation of ROMK1 H_5 had no effect on rectification, substitution of IRK1 H_5 into ROMK1 (REV. CHM A) also had no effect (Fig. 3), indicating that Mg^{2+} block

was unchanged. Rather than reducing K^+ conductance to the IRK1 value, this substitution increased g_{K^+} (48.6 ± 1.3 pS; $n = 13$). The results indicate that H_5 may play a role in determining the pore phenotype, but its contribution in IRKs is much less important than in voltage-dependent K^+ (7) and cyclic nucleotide-gated channels (10).

Because the H_5 exchanges transferred neither the Mg_i^{2+} block nor the g_{K^+} of the donor channel, more extensive exchanges were performed. The ROMK1 M_1 , H_5 , and M_2 segments were exchanged for IRK1 M_1 , H_5 , and M_2 to generate a construct named CHM B. After CHM B complementary RNA (cRNA) injection, oocytes expressed whole-cell currents having the rectification of IRK1 (Fig. 3). The CHM B construct's g_{K^+} (24.2 ± 1.3 pS; $n = 6$) was not significantly different from that of IRK1 ($P > 0.05$) but differed significantly from that of ROMK1 ($P < 0.05$). The inward rectification was due to high-affinity Mg_i^{2+} blockade (Fig. 4); at $+40$ mV, the amount of Mg_i^{2+} to inhibit the activity of CHM B by 50% (IC_{50}) was 22 μ M. The IC_{50} values

M. Tagliatela and R. Caporaso, Department of Molecular Physiology and Biophysics, Baylor College of Medicine, One Baylor Plaza, Houston, TX 77030, USA, and Department of Human Communication Science—Section of Pharmacology, 2nd School of Medicine, University of Naples “Federico II,” 5, Via S. Pansini, 80121 Naples, Italy.

B. A. Wible and A. M. Brown, Department of Molecular Physiology and Biophysics, Baylor College of Medicine, One Baylor Plaza, Houston, TX 77030, USA.

*To whom correspondence should be addressed.

for Mg_i^{2+} block of IRK1 and ROMK1 were 17 μM and 1.7 mM (18), respectively. At concentrations around the IC_{50} values, the block by Mg_i^{2+} produced a flicker in both IRK1 and CHM B channels, leading to an increase in open-channel noise. On the other hand, in ROMK1 the block resulted in a reduction of the single-channel amplitude without detectable increase in channel noise, presumably due to faster blocking rates. These kinetic properties of Mg_i^{2+} block in IRK1 are similar to those reported for native IRK channels in cardiac myocytes (11). The substitution of IRK1 M_1 , H_5 , and M_2 for ROMK1 M_1 , H_5 , and M_2 (REV. CHM B) did not result in the expression of measurable currents.

The similarities between IRK1 and CHM B channels lead to the conclusion that the structural determinants for the high-affinity Mg_i^{2+} block and the lower g_{K+}

of IRK1 reside not in M_1 , H_5 , or M_2 but in what are now described as the amino or carboxyl termini. Therefore, we asked whether one of the two termini was dominant and tested for this by exchanging each terminus separately (Fig. 2). The substitution of the amino terminus of IRK1, CHM N, produced currents having the rectification of the host ROMK1 (Fig. 3). However, the substitution of the carboxyl terminus of IRK1, CHM C, conferred strong inward rectification on ROMK1. As expected, Mg_i^{2+} block was far stronger for CHM C than for ROMK1, and the IC_{50} was 90 μM at +40 mV. CHM N had a g_{K+} of 30.1 ± 0.5 pS ($n = 5$), a value identical to that of host ROMK1. On the other hand, the g_{K+} of CHM C (26.7 ± 0.3 pS, $n = 12$) was intermediate between ROMK1 and IRK1. Thus, the carboxyl terminus is the major determinant of Mg_i^{2+} block and g_{K+} values.

Although the block by Mg_i^{2+} is voltage-dependent (13–15, 18), we do not know whether the binding site is in the membrane; allosteric coupling between the Mg_i^{2+} binding site and the pore cannot be excluded. However, if we assume that inward rectification is directly related to Mg_i^{2+} binding within the pore, then parts of the carboxyl terminus are likely to be in the membrane. Although topological models have not done so, hydrophathy plots show that there are hydrophobic stretches in the carboxyl terminus, which are potentially membrane-associated.

In voltage-dependent K^+ (7) and cyclic nucleotide-gated (10, 19) channels, H_5 appears to be a major determinant of pore function. However, several other regions may also contribute to the pore, making it a mosaic structure. In voltage-dependent K^+ channels, the S_4 - S_5 linker (20), S_6 (21–23), and a short stretch immediately be-

Fig. 3. Macroscopic currents recorded from *Xenopus* oocytes injected with cRNAs of ROMK1, IRK1, and the chimeric constructs CHM A, REV. CHM A, CHM B, CHM N, and CHM C. Holding potential, -60 mV; 100- to 250-ms steps from -100 to +40 mV in 20-mV increments; return potential, -60 mV (except in CHM B, where it was -100 mV). Dashed lines indicate zero current. Bath solutions: low K^+ -MES (filled squares); intermediate K^+ -MES (filled inverted triangles); or high K^+ -MES (filled circles). For purposes of display, part of the capacitive artifacts for the current traces of CHM A, CHM B, and CHM C have been clipped.

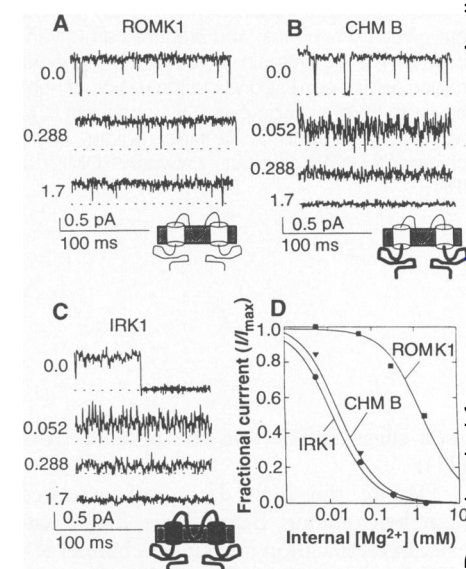
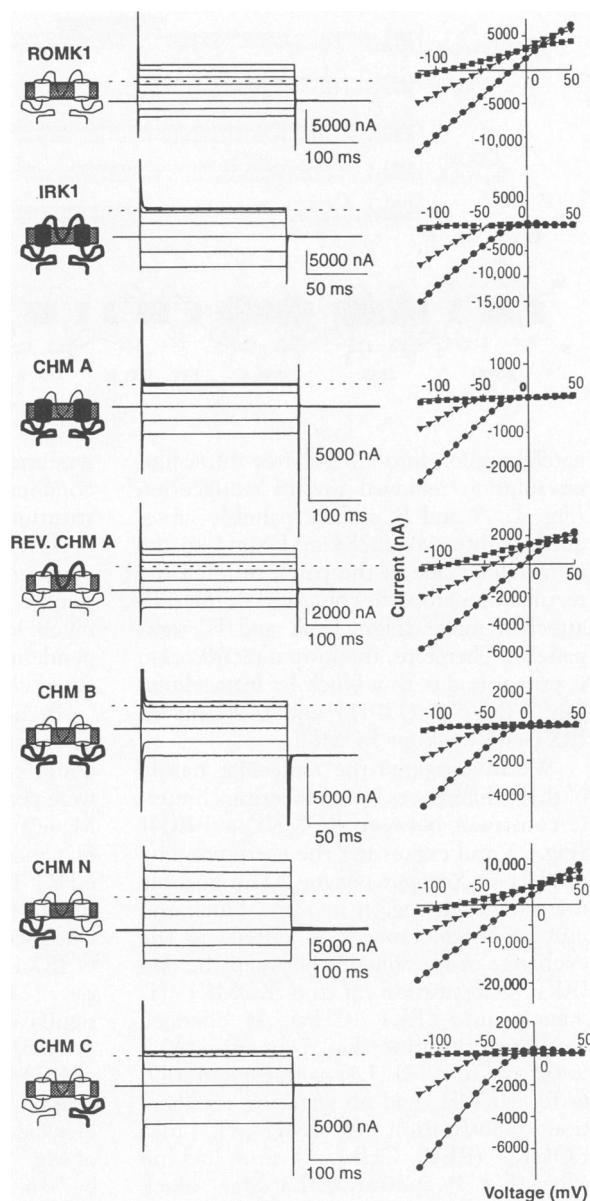


Fig. 4. Effects of internal Mg^{2+} on outward single-channel K^+ currents through ROMK1, IRK1, and CHM B. Single-channel currents from inside-out patches containing (A) ROMK1, (B) CHM B, and (C) IRK1 channels were recorded at +40 mV upon the successive exposure of the patch to concentrations of 0, 0.0052, 0.052, 0.288, and 1.7 mM free Mg^{2+} . Pipette solution, K^+ -Ringer; bath solution, iso- K^+ . (D) The single-channel current from 32 to 64 sweeps for each Mg^{2+} concentration was integrated (I), and the normalized values (I/I_{max}) were expressed as a function of the Mg^{2+} concentration. The solid lines are fits of the data from each channel to the following binding isotherm

$$y = \max/[1 + X/IC_{50}]^n$$

where X is the Mg_i^{2+} concentration and n is the Hill coefficient. The fitted value for n was between 0.8 and 1. Each data point is the average of three separate experiments. The standard error values averaged less than 15% of the mean value.

yond S_6 (23, 24) contribute to the inner mouth of the pore, while residues in the 5' region of S_6 contribute to the outer mouth (25). In IRKs, the pore seems to have a major contribution from the carboxyl terminus, with H_5 as well as M_1 and M_2 having smaller roles in K^+ conduction and inward rectification. Although the pore of IRKs may also be made up of several segments of the protein, our results call for a reassessment of the current folding model of IRK channels to account for their unique permeation and blocking properties.

REFERENCES AND NOTES

- K. Ho *et al.*, *Nature* **362**, 31 (1993).
- Y. Kubo, T. Baldwin, Y. N. Jan, L. Y. Jan, *ibid.*, p. 127.
- Y. Kubo, E. Reuveny, P. A. Slesinger, Y. N. Jan, L. Y. Jan, *ibid.* **364**, 802 (1993).
- N. Dascal *et al.*, *Proc. Natl. Acad. Sci. U.S.A.* **90**, 10235 (1993).
- D. M. Papazian, T. L. Schwarz, B. L. Tempel, Y. N. Jan, L. Y. Jan, *Science* **237**, 749 (1987); A. Baumann *et al.*, *EMBO J.* **6**, 3419 (1987); A. Kamb, L. E. Iverson, M. A. Tanouye, *Cell* **50**, 405 (1987).
- B. Tempel, Y. N. Jan, L. Y. Jan, *Nature* **332**, 837 (1988); H. R. Guy and F. Conti, *Trends Neurosci.* **13**, 201 (1990); S. R. Durell and H. R. Guy, *Biophys. J.* **62**, 238 (1992).
- H. A. Hartmann *et al.*, *Science* **251**, 942 (1991); R. MacKinnon and G. Yellen, *ibid.* **250**, 276 (1990); G. Yellen, M. E. Jurman, T. Abramson, R. MacKinnon, *ibid.* **251**, 939 (1991); A. J. Yool and T. L. Schwarz, *Nature* **349**, 700 (1991).
- M. Noda, H. Suzuki, S. Numa, W. Stuhmer, *FEBS Lett.* **259**, 213 (1989); S. Heinemann, H. Terlau, W. Stuhmer, K. Imoto, S. Numa, *Nature* **356**, 441 (1992); J. Satin *et al.*, *Science* **256**, 1202 (1992).
- S. Tang *et al.*, *J. Biol. Chem.* **268**, 13026 (1993); P. T. Ellinor *et al.*, *Nature* **363**, 455 (1993).
- E. H. Goulding, G. R. Tibbs, D. Liu, S. A. Siegelbaum, *Nature* **364**, 61 (1993).
- C. G. Nichols, *Trends Pharmacol. Sci.* **14**, 320 (1993).
- ROMK1 complementary DNA (cDNA) was obtained by reverse transcriptase-polymerase chain reaction (RT-PCR) by the use of rat kidney total RNA as template. The ROMK1 cDNA with minimal 5' and 3' untranslated sequences was subcloned into the PCR11 vector (Invitrogen, San Diego, CA) and sequenced completely in both directions. The predicted amino acid sequence is identical to the published ROMK1 sequence (2). A portion of the rat DRK1 cDNA 3' untranslated region including the polyadenylated (poly A⁺) tail was ligated to the 3' end of the ROMK1 cDNA (ROMK1-A⁺-PCR11) to boost expression of the mRNA in *Xenopus* oocytes. Chimeric cDNA constructs between ROMK1 and IRK1 were prepared by overlap extension at the junctions of the relevant domains by the use of sequential PCR [R. M. Horton, H. D. Hunt, S. N. Ho, J. K. Pullen, L. R. Pease, *Gene* **77**, 61 (1989)]. The resulting PCR products were subcloned into PCR11 and sequenced to verify the correct chimeric construction. The chimeric constructs A, B, C, and N were subcloned as Apa I-Eco RI fragments into PCR11 containing the rat DRK1 3' untranslated-poly A⁺ tail region. The reverse chimeric constructs A and B, with IRK1 regions transplanted into ROMK1, were subcloned as Apa I-Sal I fragments into ROMK1-A⁺-PCR11 from which the corresponding wild-type ROMK1 fragment had been removed. Complementary RNAs for injection into *Xenopus* oocytes were prepared by the use of the mMES-SAGE mMACHINE kit (Ambion) with T7 RNA polymerase after linearization of the plasmids with Bam H1 (for ROMK1) or Not I (for IRK1). Stage V to VI *Xenopus* oocytes were injected with 46 nl of

cRNA (2 to 100 ng/ μ l) dissolved in 0.1 M KCl [M. Tagliatela *et al.*, *Pfluegers Arch.* **423**, 104 (1993)]. Single-channel currents were recorded at room temperature (22° to 24°C) from membrane patches with fire-polished and Sylgard-coated (Dow-Corning, Midland, MI) micropipettes of 2- to 5-megohm resistance. The pipette solution was K^+ -Ringer [100 mM KCl, 2 mM $MgCl_2$, 10 mM Hepes (pH 7.3)], while the bath solution was iso- K^+ [100 mM KCl, 10 mM EGTA, 10 mM Hepes (pH 7.3)]. $MgCl_2$ was added to the bath solution to give calculated concentrations of free Mg^{2+} ions [A. Fabiato and F. Fabiato, *J. Physiol. (Paris)* **74**, 463 (1979)]. Data were low-pass filtered at 1 to 2 kHz (-3 dB, 4-pole Bessel filter) before digitization at 5 to 10 kHz. The pClamp software (Axon Instruments) was used for the generation of the voltage-pulse protocols and for data acquisition. Ramp-stimulated currents (0.5 to 2 mV/ms) were analyzed as described [G. E. Kirsch *et al.*, *Biophys. J.* **62**, 136 (1992)]. Macroscopic currents were recorded with a conventional two-microelectrode voltage-clamp technique [M. Tagliatela *et al.*, above]. For macroscopic current recordings, bath solutions were as follows: low K^+ -MES [2.5 mM KOH, 120 mM *N*-methyl-D-glucamine, 122.5 mM MES, 2 mM $Mg(OH)_2$, and 10 mM Hepes (pH 7.3)]; intermediate K^+ -MES [22.5 mM KOH, 100 mM *N*-methyl-D-glucamine, 122.5 mM MES, 2 mM $Mg(OH)_2$, and 10 mM Hepes (pH 7.3)]; or high K^+ -MES [100 mM KOH, 22.5 mM *N*-methyl-D-glucamine, 122.5 mM MES, 2 mM $Mg(OH)_2$, and 10 mM Hepes (pH 7.4)]. Statistical analysis was performed by means of the two-tailed Student's

- t* test for samples of unequal variances.
- H. Matsuda, A. Saigusa, I. Irisawa, *Nature* **325**, 156 (1987).
- C. A. Vandenberg, *Proc. Natl. Acad. Sci. U.S.A.* **84**, 2560 (1987).
- K. Ishihara, T. Mitsuye, A. Noma, A. M. Takano, *J. Physiol. (London)* **419**, 297 (1989).
- H. Matsuda, *ibid.* **397**, 237 (1988).
- M. R. Silver and T. E. DeCoursey, *J. Gen. Physiol.* **96**, 109 (1990).
- C. G. Nichols, K. Ho, S. Hebert, *Proc. Physiol. Soc.* **1993**, 46 (1993).
- M. J. Root and R. MacKinnon, *Neuron* **11**, 459 (1993).
- E. Y. Isacoff, Y. N. Jan, L. Y. Jan, *Nature* **353**, 86 (1991); P. A. Slesinger, Y. N. Jan, L. Y. Jan, *Neuron* **11**, 739 (1993).
- G. E. Kirsch, C.-C. Shieh, J. A. Drewe, D. F. Verner, A. M. Brown, *Neuron* **11**, 503 (1993).
- K. L. Choi, C. Mossman, J. Aube', G. Yellen, *ibid.* **10**, 533 (1993).
- G. A. Lopez, Y. N. Jan, L. Y. Jan, *Nature* **367**, 179 (1994).
- M. Tagliatela *et al.*, *J. Biol. Chem.*, in press.
- T. Hoshi, W. N. Zagotta, R. W. Aldrich, *Neuron* **7**, 547 (1991).
- We thank L. Jan for providing the IRK1 clone; W.-Q. Dong for injecting and handling oocytes; T. Afinni, C. Zhu, S. Dou, and S. Pan for expert molecular biology support; and G. E. Kirsch and A. E. Lacerda for helpful comments. Supported by NIH grants NS23877, HL36930, and HL37044 (A.M.B.).

31 January 1994; accepted 21 March 1994

Neural Tuning for Sound Duration: Role of Inhibitory Mechanisms in the Inferior Colliculus

J. H. Casseday,* D. Ehrlich, E. Covey

Duration is a biologically important feature of sound. Some neurons in the inferior colliculus of the big brown bat, *Eptesicus fuscus*, are tuned to sound duration, but it is unclear at what level the tuning originates or what neural mechanisms are responsible for it. The application of antagonists of the inhibitory neurotransmitters γ -aminobutyric acid or glycine to neurons in the inferior colliculus eliminated duration tuning. Whole-cell patch-clamp recordings of synaptic currents suggested that inhibition produces a temporal frame within which excitation can occur. A model is proposed in which duration tuning arises when an early, sustained inhibitory input interacts with a delayed, transient excitatory input.

The duration of a sound is a signature of biological importance, particularly in speech or echolocation signals. The perception of speech patterns, including the silent gaps between sounds, operates within time constraints in such a way that the same sounds are perceived differently, depending on their duration (1). The signals emitted by echolocating bats vary in duration according to the phase of hunting in which the bat is engaged. The big brown bat systematically varies the duration of its echolocation call during pursuit of flying prey; the longest signals (up to 20 ms) occur in the initial or "search" phase, and the shortest signals (<1 to 2 ms) occur during the "approach" phase (2). The mechanism

for neural representation of sound duration is not simply one in which neurons respond throughout the sound, because most auditory neurons above the lower brainstem respond transiently (3).

Although duration-tuned neurons are found in the inferior colliculus of bats (4), present evidence is not sufficient to rule out the possibility that duration tuning is generated at an earlier stage. The inferior colliculus is an integration center that receives the parallel inputs of auditory pathways from the lower brainstem (5, 6). The prominence of inhibition in the inferior colliculus (7) suggests that duration tuning is controlled by neural inhibitory mechanisms. However, there has been no evidence to support this idea. This report provides evidence that duration tuning is constructed in the inferior colliculus through the interaction of excitatory and

Department of Neurobiology, Duke University Medical Center, Durham, NC 27710, USA.

*To whom correspondence should be addressed.